Exp. Theo. NANOTECHNOLOGY 10 (2026) 925-944 https://doi.org/10.56053/10.S.925

Characterization of Cu-Ni multilayers coating by electroplating on carbon steel A106 grade C used for petroleum applications

Maryam Abdulameer Ali[*], *Israa A. Aziz*, *Ahmed Salloum Abbas*

Production Engineering, and Metallurgy College, University of Technology- Iraq, Baghdad, Iraq
[*]) Email: pme.24.05@grad.uotechnology.edu.iq

Received 1/2/2026, *Received in revised form* 1/4/2026, *Accepted* 15/4/2026, *Published* 15/5/2026

Low carbon steel is extensively employed industrial pipelines due to its low cost, and eases of welding, but its susceptibility to corrosion necessitates surface protection strategies such as: electroplating (ELP). In this study, multiple layers of copper (Cu) and nickel (Ni) are deposited on a low carbon steel type A106 grade C (St.A106-B) substrate using the (ELP) process. The samples are divided for coating into three groups: the first group is Ni coating layer, the second is Cu coating layer, and the third consisted of two layers, Cu and Ni. The experiments are conducted over three different electroplating periods: 10, 20, and 30 minutes (min.). The parameters, including the ELP time, are studied in the experiments. Measurement and tests methods are used , which included roughness, micro hardness testing, thickness measurement, and X-ray diffraction (XRD) analysis to describe the multilayers phases features compared to all obtained samples, also surface compositions of the electroplated layers are calculated using these methods. Results have been showed that surface roughness, thickness, and hardness increase, with increasing the ELP time. The obtained results indicate that increasing the electroplating time will lead to an increase in the thickness of the coating layer. On the other hand, increasing the electroplating time affected the increase in surface roughness of both Ni and Cu. The highest value of microhardness is achieved at the longest plating time in the Cu-Ni bilayer (30 min.). As for the XRD test results, consider as good evidence of the presence of Cu, Ni and Cu-Ni in both the inner and outer finishing layers, respectively.

Keywords: ELP; Mmultilayer; Surface roughness; Low carbon steel A106.

1. INTRODUCTION

Due to the growing demand for advanced and new materials in many engineering applications, increasing research efforts have been directed toward surface engineering techniques aimed at imparting enhanced and tailored surface properties that differ from those of the bulk substrate [1-5]. Electroplating, which is an electrochemical deposition process, produces dense, uniform, and adherent metallic or alloy coatings on substrates through the application of electric current [6-10]. These coatings are widely used for decorative and protective purposes to enhance surface performance [11-15]. Over the past five decades, Ni electroplating technology has seen significant development, enabling the efficient production of a wide range of industrial coatings for engineering applications [16-20].Ni coatings are known to improve fundamental physical and mechanical properties, including corrosion resistance, wear resistance, thermal stability, and chemical durability [21-25]. In many applications, these coatings provide a glossy and aesthetically appealing finish while simultaneously enhancing resistance to chemical attacks and other environmental degradation mechanisms. Ni-Cu coatings are widely used to enhance the durability and corrosion resistance of industrial components [26-30]. In multi-layer Ni-Cu systems, Ni acts as a protective underlayer for pipes, valves, pumps, and mechanical parts exposed to harsh environments, while Cu is often used as an intermediate layer to improve adhesion and provide additional corrosion protection [31-35]. These multi-layered coatings are particularly effective in oil and gas, marine, and chemical processing applications, where resistance to carbon dioxide, hydrogen sulfide, and saline conditions is critical [36-40]. Preparation for the ELP process involves thoroughly cleaning the surface intended for plating from organic materials such as: grease and oils, which can be removed using conventional solvents or by cleaning with alkaline substances or inorganic chemicals like oxides [41-45]. ELP offers many benefits due to its simplicity and ease of control, as well as being environmentally friendly and involving low material consumption, making it economically feasible in addition to providing surface protection [46-50]. The ELP mechanism involves three stages [51-55]. The first stage is the discharge of metal ions to form adsorbed atoms, which move toward the cathode under the influence of the applied voltage through convection and diffusion [56-60]. The second stage includes the transfer of electrons on the cathode surface to enter the diffusion and adsorption layer on the cathode surface [61]. The third stage, known as the incorporation stage, involves transferring these adsorbed atoms to the growth sites on the cathode to build the metallic lattice layer and controlling all of these variables can improve the coating process [62, 63]. The effect of plating process variables such as: current density, plating time, and composition of the electrolyte solution, and it observed that the best Ni deposition occurred at 0.5 V for 15 min in a bath, with a concentration of 4.18 mol/dm^3, which improved the quality of the Ni ELP on low carbon steel [64]. The results indicated that optimizing these variables significantly enhances the thickness and surface uniformity while improving the mechanical properties, which in turn boosts corrosion resistance [13]. The process of electroplating copper onto low carbon steel using alkaline solutions [14] composed of citrates found that citric acid baths with a concentration of 0.1 mol/dm^3 of copper sulfate $CuSO_4$, and 0.5 mol/dm^3, and with a pH ranging between 9 - 11, are optimal for obtaining a coherent and uniform copper layer, focusing on the composition of the solution and deposition conditions to achieve homogeneous and coherent layers. The experiment showed that citrate-based solutions produce a stable copper deposition while improving the shape and quality of the coating surface and thereby reducing hydrogen evolution compared to conventional acidic solutions [14]. Many researchers have been focusing on protecting low carbon steel, with conventional or nanocoating methods [15]; Kadhim et al. [16] have investigated the impact of zinc oxides nanoparticles (ZnO_{NP}) via pulse laser deposit PLD on pipeline steel Type A106 Grade B, the results show a good enhancement in corrosion protection for this pipeline steel. Abbas, et al studying the

effect of ZnO_{NP} coated on steel type 37 grade 2 (ST37-2) using PLD, this type of steel using in Oil storage applications the implanted PLD technique offer a good corrosion protection [17]. Low carbon steel coated, with Ni is studied by Salih et al. Through stresses tests, weight loss measurements due to corrosion, and microstructure examination to evaluate performance in corrosive environments. Five sets of standard low carbon steel samples are prepared for fatigue tests, and then mechanical grinding is performed on all 45 samples. After that, ELP with Ni is carried out on 18 samples, and mechanical polishing is performed on the remaining 27 samples. The enhanced nickel coating resulted in an increase in fatigue life by about 30–50%, a reduction in corrosion rate by about 40%, and an improvement in surface hardness compared to the uncoated substrate [18]. Abdulhussein et al. [19] have fabricated a nano silica thin film SiO_2 using sand as sources plated on carbon steel type A285 grade C in order to reducing corrosion attacks this type of steel used on in petroleum storage tanks.in this work the properties of Ni-Cu multilayer ELP on a St. A106 - B substrate is studied.

2. EXPERIMENTAL PROCEDURE

2.1. Substrate geometry

St. A106-B substrates are cut into rectangular shapes measuring 20 × 20 × 4.5 mm using a water jet machine. To enable the samples to be hung in the electroplating bath, a 2 mm hole is drilled in each. The geometry of the samples utilized in this research is depicted in Figure 1.

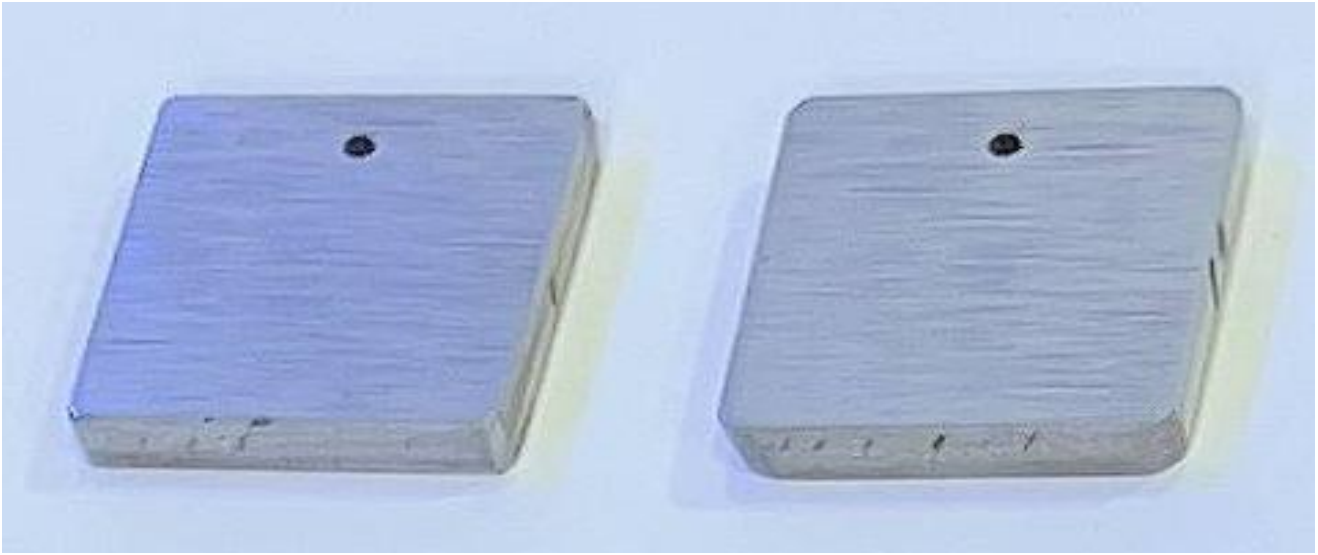

Figure 1 The geometry of St.A106-B samples.

2.2. Chemical analysis of low carbon steel

The chemical composition analysis of St. A106-B is conducted at General Company for Testing and Rehabilitation of Electrical Power Systems using a Q_4 Mobile Optical Emission Spectrometer (OES), a robust mobile model manufactured in Germany, as shown in Figure 2. The testing conditions are temperature kept between 23-25 °C and the humidity range 65-67%. The results of the analysis are illustrated in the Table 1, which, include the stander and actual measured values.

Table 1 Results of chemical composition analysis for low carbon steel A106 grade C.

Chemical composition %	Standard values	Actual values
C%	0.25	0.235
Si%	0.35	0.222
Mn%	0.90	0.435
Cr%	0.40	0.036
Mo%	0.15	0.019
Ni%	0.40	0.036
Cu%	0.20	0.110
Al%	-	0.017
Co%	-	< 0.0100
Nb%	-	< 0.0100
V%	0.08	< 0.0050
W%	-	< 0.030
Ti%	-	<0.0020
Zr%	-	< 0.0050
Fe%	The rest	98.88

Figure 2 Mobile Optical Emission Spectrometer (OES).

2.3. Preparation for low carbon steel substrate tests

For microstructural examinations and hardness testing, a sample of low carbon steel must be prepared. The following steps are followed in this work. First, low carbon steel samples are cut into small pieces with dimensions of (2×2) cm. Second, the samples are mounted using cold mounting to facilitate handling during preparation processes such as grinding, polishing, and chemical etching. Cold mounting is carried out by mixing the hardener and resin.

2.4. Examination of the microstructure of low carbon steel

The microstructure is examined through three steps. First, the samples are grinding using sandpaper with different grit sizes ranging from 120 to 2000. Second, the samples are polished using a soft cloth saturated with abrasive aluminum oxide particles with a lubricant; adhesive is also added until the sample surfaces become mirror-like. The microstructure is observed using an optical microscope (Carl Zeiss Jena) connected to a digital camera controlled by a computer. The results showed dark areas indicating the pearlite phase (P), while the light areas correspond to the ferrite phase (α), as shown in Figure 3. This test is carried out in the Production Engineering and Metallurgy College at the University of Technology, Baghdad.

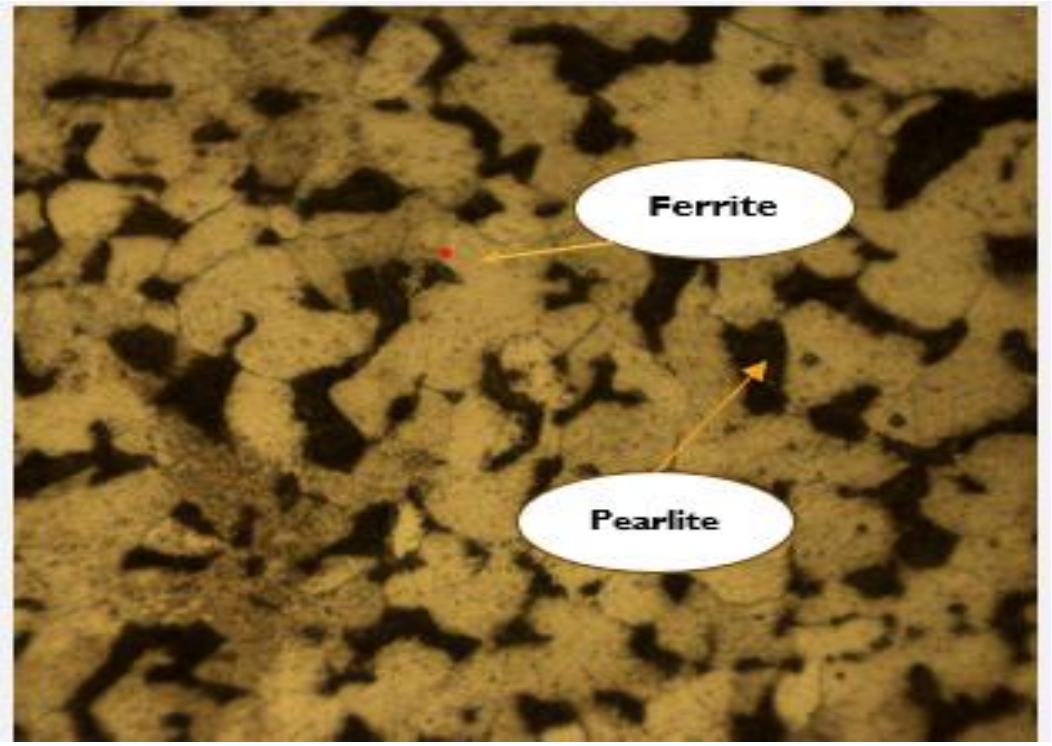

Figure 3 low carbon steel A106 G-C microstructure (100 x).

2.5. Vickers hardness test

The hardness of all prepared samples before and after coating is determined using a Vickers hardness device, model (TH714) available at Production Engineering and Metallurgy college. The applied force is 100 grams (gm). The time for this applied force is 15 second (sec.), so the calculation of the Vickers hardness (Hv), is given by the equation [4,65-67]:

$$Hv=1.8544\times P/ (dav)^2 \quad (1)$$

where Hv: Vickers hardness (kg/ mm²), dav.: Arithmetic mean of the diagonal lengths of the indentations (mm) and P: applied load (kg).

2.6. Preparing samples for ELP

The surface of the samples to be coated must be cleaned. These preparation activities include cleaning and rinsing with water to remove dirt, defects, and grease remaining from production processes. This process ensures optimal adhesion between the metal substrate and the coating layer. To achieve an electroplating process with good properties, an electroplating cleaning cycle is carried out in four steps:

1. Hot alkaline cleaning by immersing the samples in a bath containing a hot solution of (NaOH).
2. Rinsing with distilled water.
3. Acid cleaning by immersing the samples in a bath containing a diluted solution of hydrochloric acid (HCl).
4. Rinsing with distilled water. and direct electroplating, immersing the samples in the bath for (10, 20, and 30 min.), respectively.

2.7. Thickness test

The thickness of the coating layer is measured using the cross-sectional cutting method of the sample. The samples are then mounted, polished, smoothed, and etched using an etching solution so that the thickness can be measured using an optical microscope in the laboratories of Production Engineering and Metallurgy college at the University of Technology, Baghdad.

2.8. Roughness inspection

The surface roughness of coated metals is measured using a portable surface roughness tester of the type (Pocket Surf) manufactured by Mahr Federal Inc., USA, with an accuracy of up to (0.001µm). These tests are carried out in the measurement laboratory at the Faculty of Production and Metallurgical Engineering. Figure 4 shows the setup of the surface roughness testing device with the sample.

Figure 4 The surface roughness device.

3. MATERIALS AND EQUIPMENT

3.1. Cu ELP

To carry out the ELP process, the necessary equipment and materials must be available, including: square samples with dimensions (20 × 20 × 4.5 mm.). The samples are drilled with a diameter of (1.5 mm.) at the center at the top of the sample for suspension purposes. The components of the electroplating bath include $CuSO_4 \cdot 5H_2O$, H_2SO_4, and $Cu(BF_4)_2$, and this bath is made of plastic that does not react with the bath components. Cu electrodes (rods), with a purity of over 95% are used, along with Cu holders to hold the sample in the bath during the plating process. Distilled water is used. Equipment such as a power supply, an electric heater, with a power of (1500) watts, a digital voltmeter to measure voltage, and finally an ammeter to measure current are also used. Table 2 illustrates the conditions of the copper electroplating process.

Table 2 Cu ELP process conditions.

Electroplating Conditions	Standard Parameters	Actual Parameters
Temperature of electroplating	50-60 ^oC	**45** ^oC
pH	9-11	9
Size of bath	100 liter	50 liter
Sample size	-	2*2*0.42 cm
Electroplating time	-	10-30 min.
Area of anode to cathode	2-1	2-1
Current density	-	2amp/dcm^2
Voltages	6-12 V	(9-5) V
Cathode and anode distance	Max. 25 cm	5 cm

The ELP process began by drilling holes in the samples, connecting Cu wires to them, and attaching them to the cathode while the Cu is connected to the anode. The sample is then immersed in the electrolyte solution. The appropriate electric current is passed through the solution to reach a stable state and to obtain a good coating layer. The temperature of the bath is controlled using a thermometer, within the required range, and the pH value is measured, which is found to be (9). Figure 5 shows the samples after electroplating with different layers (Cu, Ni, Cu-Ni). The voltage is also measured using a voltmeter during plating, with a plating voltage of 5, 6, and 9 V. Plating is carried out over time periods of 10, 20, and 30 min. On the other hand, the surface of the copper coating layer is examined using an optical microscope. Figure 6 illustrates the morphology of the Cu coating deposited on low carbon steel. The Cu surface appears smooth and uniform, indicating that a good Cu coating has been achieved [68-71].

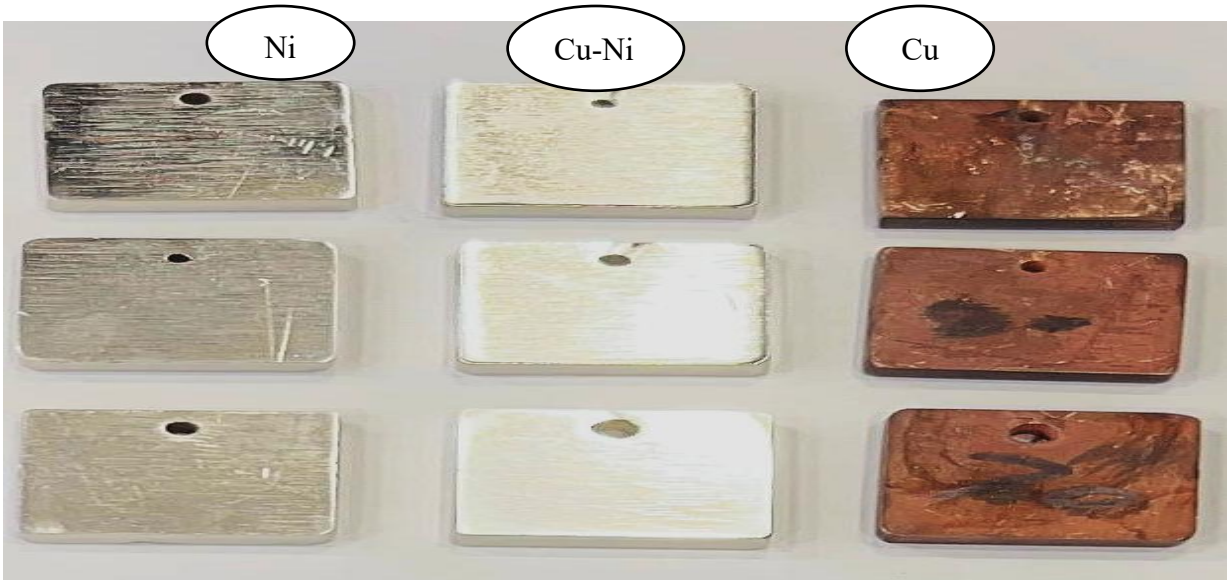

Figure 5 The samples after ELP, with different layers (Ni, Cu, Cu-Ni).

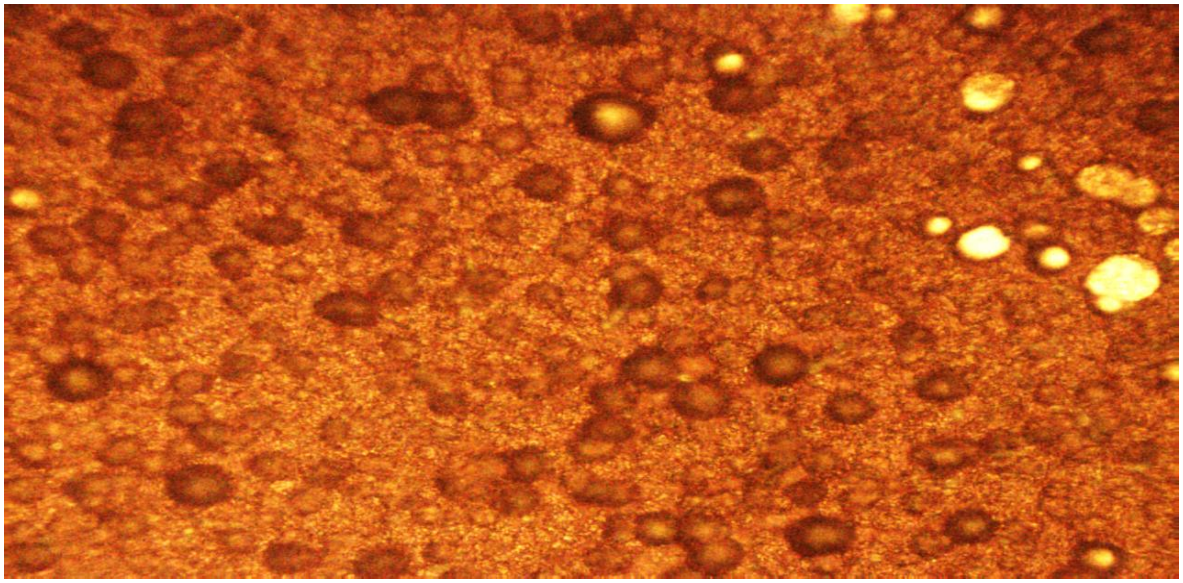

Figure 6 The morphology of the Cu coating deposited on low carbon steel, with 30 min. 400x.

3.2. Ni ELP

For the same previous square samples, the plating process is carried out this time using Ni, where a Ni layer is obtained using a rectangular plating cell (50 liters) containing (30 g/L) of $NiSO_4 \cdot 6H_2O$, (30 g/L) of $NiCl_2 \cdot 6H_2O$, and (40 g/L) of H_3BO_3 under applied current plating conditions (10 amp/dcm^2) and plating durations of (10-20-30 min); meanwhile, the samples after Ni electroplating are shown in Figure 7, with a shiny, bright, mirror-like surface Table 3 illustrates the conditions of the Ni ELP process [72, 73].

Table 3 Ni ELP process conditions.

Electroplating Conditions	Standard Parameters	Actual Parameters
Temperature of electroplating	60-65 ℃	65 ℃
pH	9-11	4.5
Size of bath	100 liter	50 liter
Sample size	-	2*2*0.42 cm
Electroplating time	-	10-20-30 min.
Area of anode to cathode	2-1	2-1
Current density	-	10amp/dcm²
Voltages	6-12 V	12 V
Cathode and anode distance	Max. 25 cm	5 cm

The (ELP) process began by making holes in the samples and connecting them to the negative electrode using Cu wires, while the Ni is connected to the positive electrode. The samples are then immersed in the electrolyte solution, and the appropriate current is applied to the electrolyte for plating to achieve a stable state and form a good coating layer. The bath temperature is controlled using a thermometer, and maintained within the desired range, while the pH is measured to be 4.5. The voltage is monitored during ELP using a voltmeter and is 12 V. The plating process is carried out for different durations of 10, 20, and 30 min. After Ni ELP, the surface of the Ni layer is examined using an optical microscope [74-76]. The resulting surface topography of the Ni layer, as shown in Figure 7, displayed a smooth and uniform layer on low carbon steel, indicating successful nickel deposition.

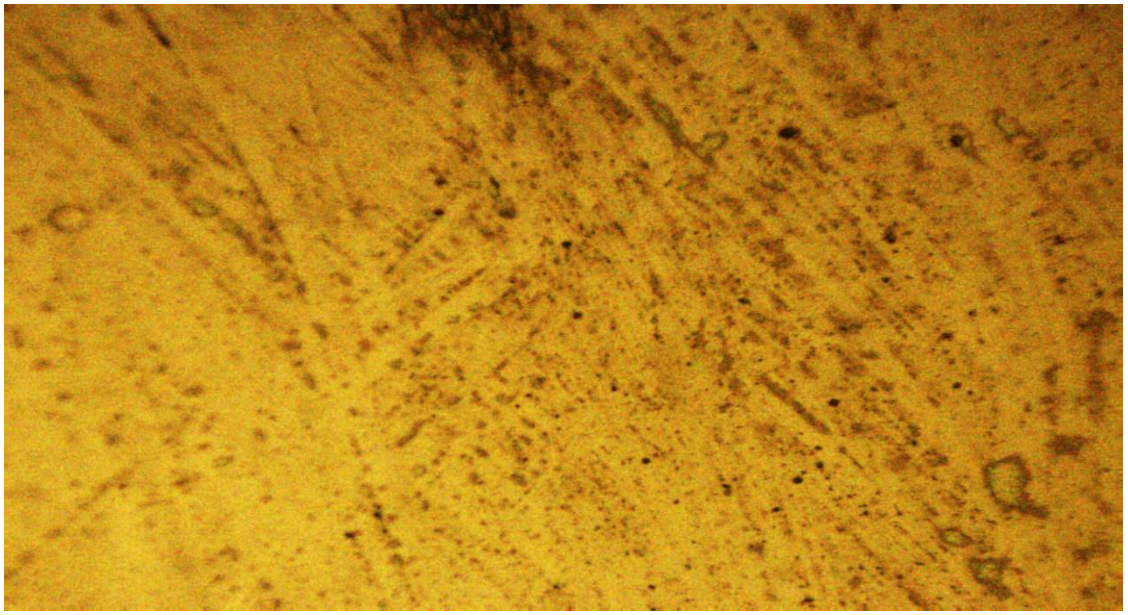

Figure 7 The morphology of the Ni coating deposited on low carbon steel with 30 min. 400x.

3.3. Cu – Ni ELP

The third group, shown in Figure 8, included a two-layer coating consisting of a layer of Cu followed by a layer of Ni, with a coating duration of 10-20-30 min. The previous steps are repeated under the

same conditions for the coating layers, and the properties are subsequently studied, as will be presented sequentially [77-80]. Figure 8, displayed a smooth and uniform deposition on low-carbon steel, indicating successful Cu- Ni deposition.

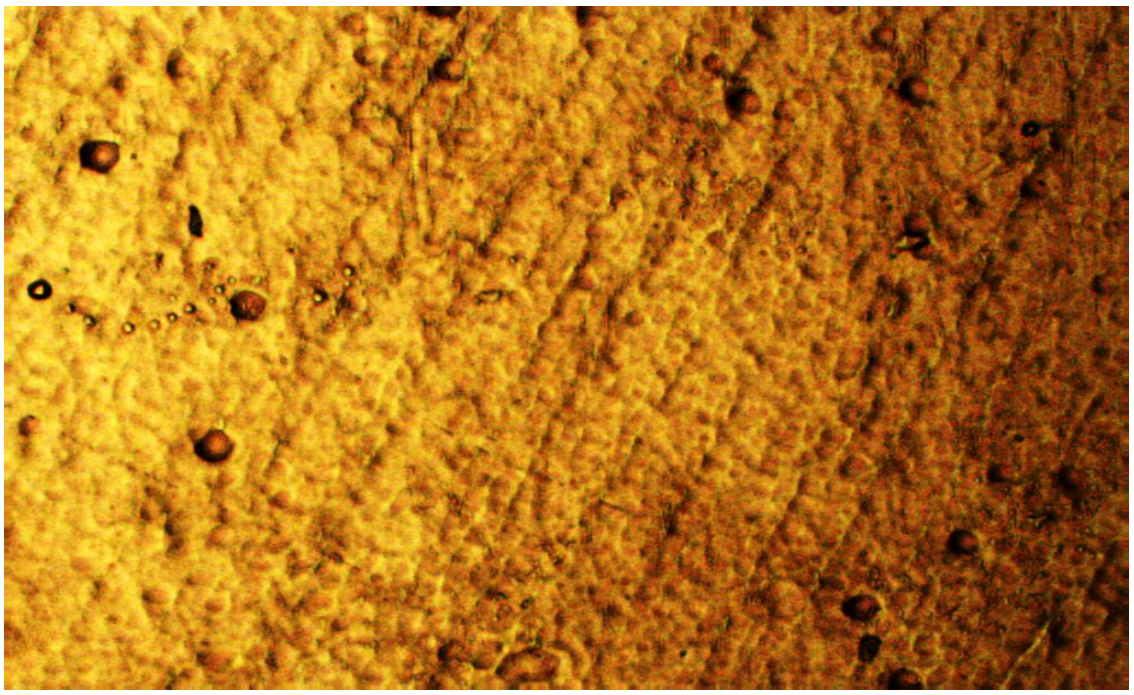

Figure 8 Cu- Ni deposition with 30 min 100x.

4. RESULTS AND DISCUSSION

4.1. ELP thickness

The experiment showed the effect of plating time on the thickness of Cu and Ni coating layers under the conditions in which the plating process is carried out, where both elements had nearly constant conditions of temperature, current density, and solution concentration. The highest thickness of Cu coating on a low-carbon steel substrate is achieved at 30 min, reaching a thickness of 23.6 µm with a current of 2 amps, a voltage of 5 V, and a temperature of approximately 45 ℃. At the same time, the maximum thickness of the Ni coating on the same base metal is achieved after 30 min, reaching a thickness of 35.4 µm using a current of 10 amps, a voltage of 12 V, and a temperature close to 65 ℃. As for the Cu-Ni coating, its highest thickness is also reached in 30 min, amounting to 52.4 µm, which means that the greater the deposition time, the thicker the coating [16, 81-85]. Figure 9 illustrates the relationship between the copper thickness, nickel thickness, and coating duration.

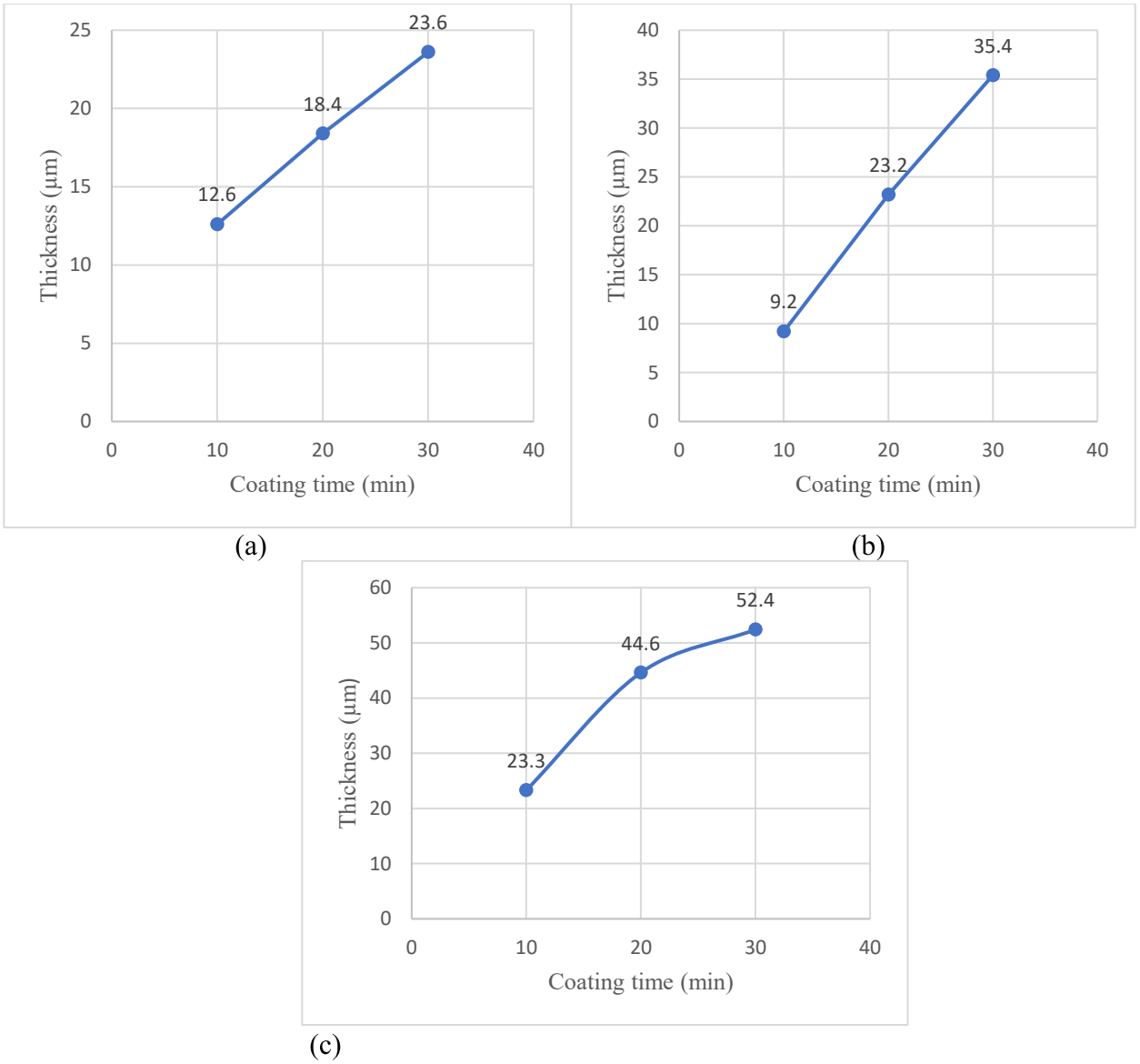

Figure 9 The relationship between the ELP thickness of (a) Cu, (b) Ni, (c) Cu-Ni and the plating time.

4.2. Surface roughness

The topographical properties of the coating layer surface (Ni and Cu) are influenced by the varying factors in the electroplating process, such as current density, temperature, solution concentration, and plating duration. Figure 10 illustrates the relationship between the average surface roughness of Ni and Cu and the electroplating time. It is observed that roughness values increase with increasing plating time, reaching the highest average surface roughness values of (0.93 µm) for Cu and (0.97 µm) for Ni at a plating duration of (30 min), while for the bilayer coating (Cu-Ni) the roughness reached (0.09 µm), indicating that intermediate copper layers reduce roughness values [86, 88]. On the other hand, the effect of electroplating thickness on surface roughness is directly proportional to the increase in plating time [17].

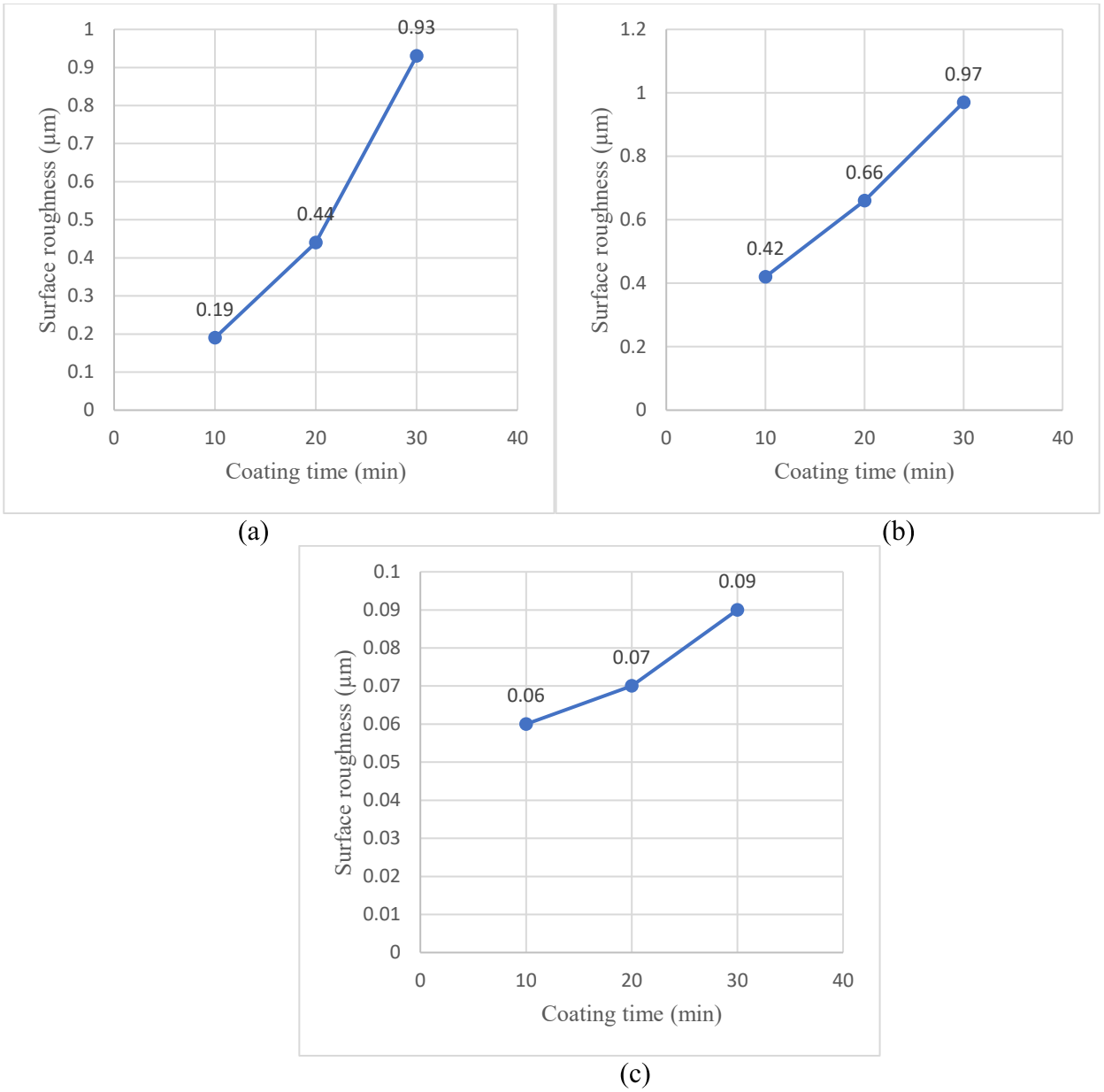

Figure 10 The relationship between the surface roughness and the electroplating time (a)Surface of Cu roughness (b) Surface of Ni roughness (c) Surface of Cu-Ni roughness.

4.3. Microhardness after electroplating

Figure 11 illustrates the hardness values obtained for the samples coated with Cu, Ni, and Cu-Ni coatings at different plating times applied to low-carbon steel samples using ELP. The coatings are deposited for (10, 20, and 30 min) under a load of 100 gm, and the hardness is measured using the Vickers hardness test (Hv). In figure 11 (a) the hardness of the Cu layer at different times is shown the difference in the measured hardness of the base metal and the copper layer is due to differences in properties and crystalline structure, as steel is an alloy of iron and carbon, where the small carbon atoms hinder the sliding of iron atomic layers, and this is the reason for its relatively high resistance to

deformation compared to Cu, which has a single crystalline structure and is malleable, and ductile, making it classified as easy to shape and soft compared to steel [18,19].

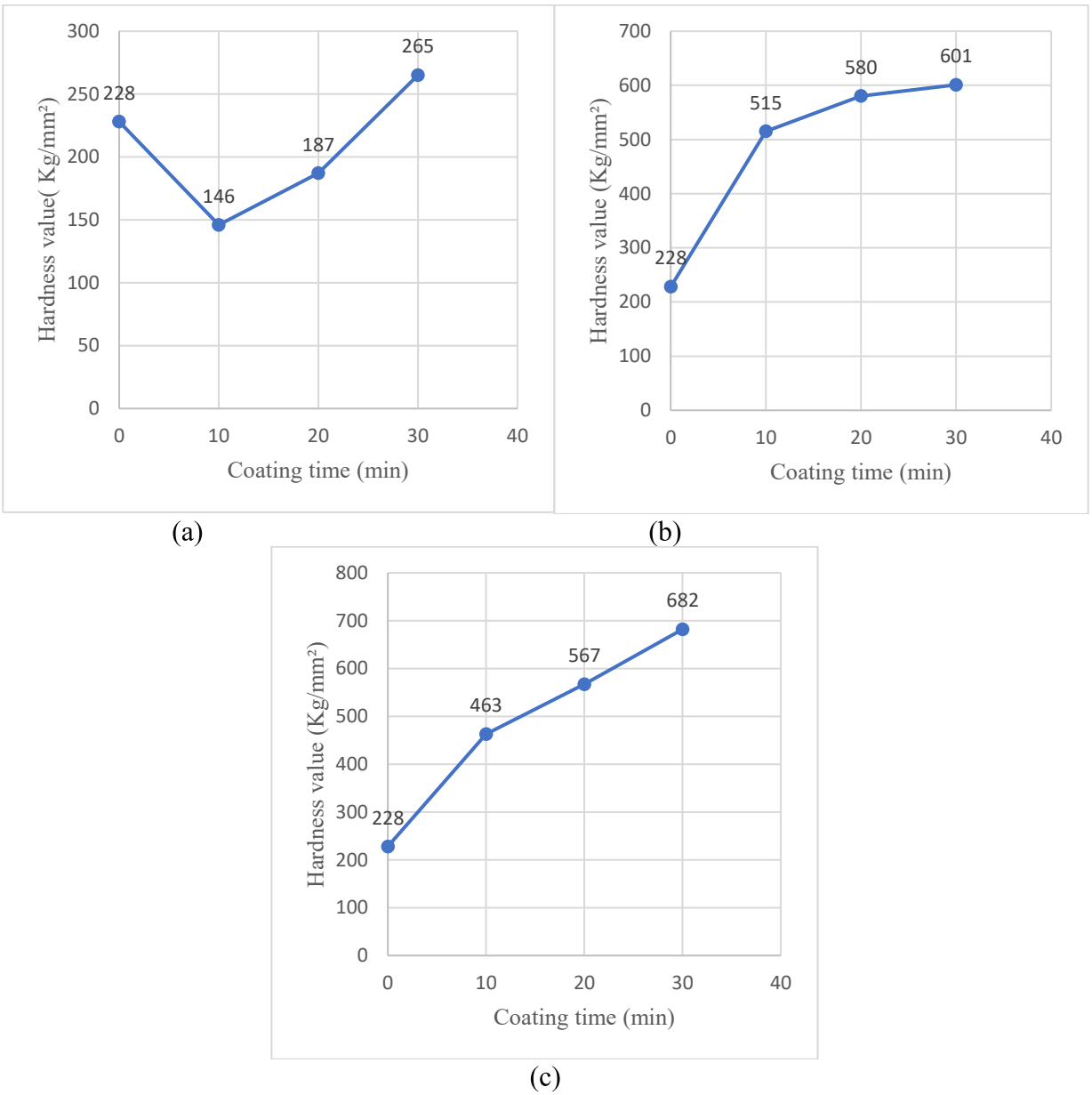

Figure 11 The hardness values for (a) Cu layer (b)Ni layer (c)Cu-Ni layer.

The hardness of untreated low carbon steel is 228 Hv, representing the baseline value, as this type is characterized by more flexibility and durability compared to hardness. After Ni plating, the hardness increased to 601 Hv, indicating that Ni significantly enhances surface hardness and improves durability and corrosion resistance. As for Cu plating, the hardness increased to 265 Hv after 30 min of plating for the previously mentioned reason, which is a slight improvement compared to the uncoated metal, and is much less than the effect of Ni. Regarding the double coating Ni-Cu, it gave 682 Hv, which is much higher than Cu and slightly more than Ni alone, due to the interaction between the two metals and its effect on the microstructure [89, 90]. In general, all coatings improved hardness compared to the uncoated sample, and the double Cu-Ni coating is the most effective [20].

4.4. XRD analysis

The X-ray diffraction (XRD) patterns of Cu and Ni ELP on low-carbon steel via an ELP bath at a pH value of 4.5 for Ni and 9 for Cu, and current densities of 10 A/dm² and 2 A/dm² respectively, for (10-20-30 min), and at temperatures of 65-45°C are shown in Figure 12. The XRD analysis of the coating shows a strong diffraction peak at 44.63°, 64.95°, and 82.24° in black with planes (011), (002) and (112) respectively, belonging to the low-carbon steel substrate As shown in the three patterns illustrated in the figure 12.Meanwhile, the other peaks of the coatings at 30 min, appearing as the most intense in pattern(a), indicate the copper coating on the substrate with variations in broad peaks at 43.29°, 50.41°, 74.07°, and 89.87° with planes (111), (002), (022) and (113) respectively .On the other hand, the XRD in pattern (b) shows strong peaks belonging to Ni at 44.49°, 51.85°, and 76.38° with planes (111), (200) and (220) respectively. For the Cu-Ni coating, the XRD in pattern (c) shows strong peaks belonging to Cu-Ni at 42.95°, 50.02°, 73.43°, and 89.03° with planes (111), (002), (022) and (113) respectively [21]. Moreover, the difference between the broad peaks of one plane and another for the Cu-Ni coating is an indicator of the presence of multiple layers of Cu-Ni on low carbon steel, which is evident in the figure below [91-95].

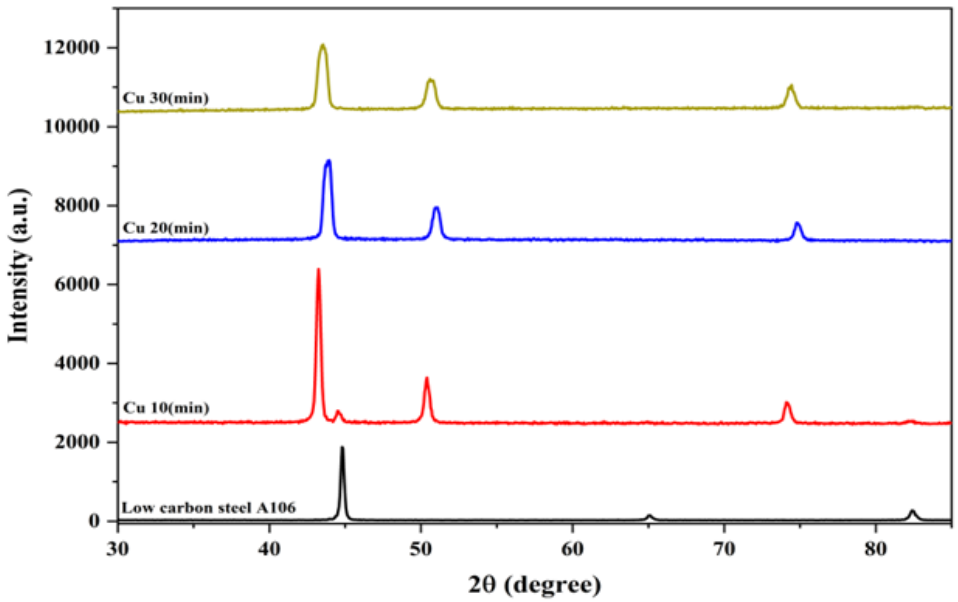
Cu 30(min)
Cu 20(min)
Cu 10(min)
Low carbon steel A106
Intensity (a.u.)
2θ (degree)
12000
10000
8000
6000
4000
2000
0
30
40
50
60
70
80

(a)

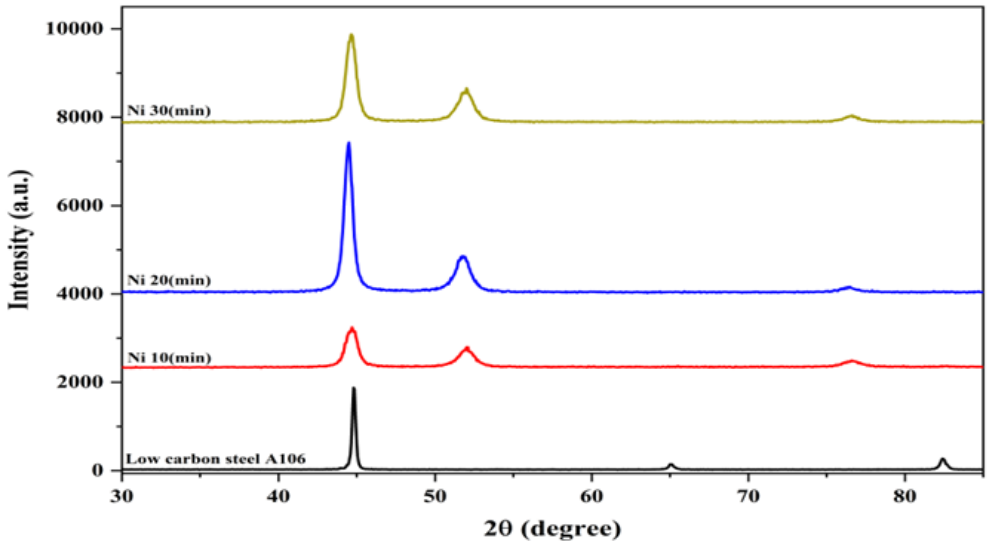
Ni 30(min)
Ni 20(min)
Ni 10(min)
Low carbon steel A106
Intensity (a.u.)
2θ (degree)
10000
8000
6000
4000
2000
0
30
40
50
60
70
80

(b)

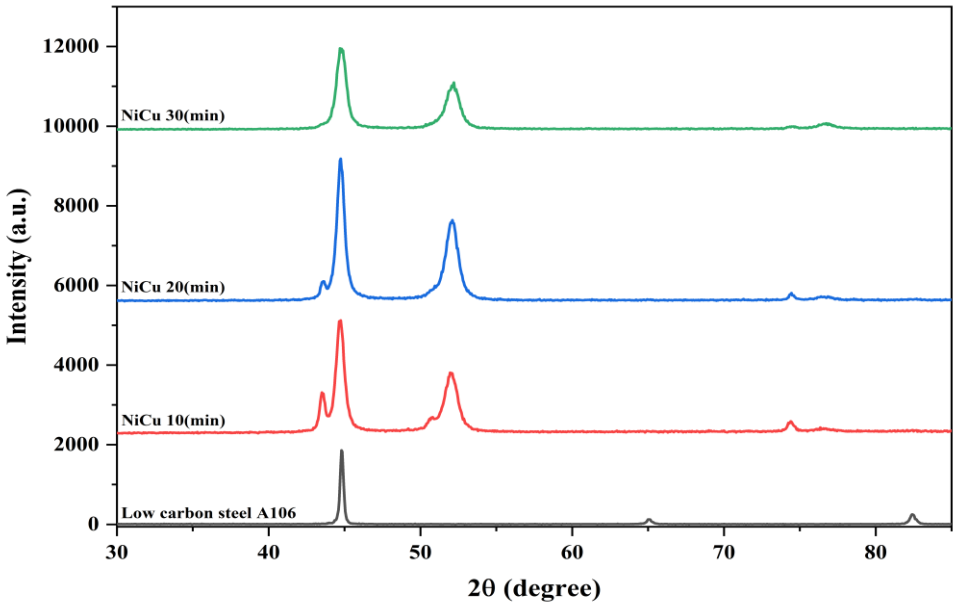

(c)

Figure 12 The XRD pattern after ELP (a) Ni (b)Cu (c) Cu-Ni coating.

4.5. SEM and EDX analysis

Superficial images of the coatings for both Cu and Ni and Cu-Ni appear with a time of 30 min, as is evident from Figure 13. We start with image (a) showing the surface morphology (SEM)The scanning electron microscope image reveals a dense, fine, and protruding structure (resembling cauliflower), which is typical of electrodeposited Cu. The coating is continuous and uniform on a 25 μm scale, with no obvious cracks or large porosity, indicating a well-adhered coating layer. Chemical composition (EDX): EDX analyses confirm that the deposited layer is mainly composed of Cu (96.6 wt%), indicating high purity. The presence of oxygen (2.5 wt%) is attributed to slight surface oxidation upon air exposure. Small amounts of Ni (0.5 wt%) and Fe (0.4 wt%) are also detected, likely resulting from minor impurities in the electrolyte or signal penetration from the substrate. The SEM image (b) micrograph shows smooth and homogeneous surface with only minor surface irregularities and a few small protrusions. The absence of large nodular structures indicates that the deposited layer possesses a fairly uniform morphology, suggesting stable ELP conditions during deposition. The EDS analysis confirms that the coating is predominantly composed of Ni, with a high concentration of approximately 98.5 wt% Ni, indicating successful Ni deposition and good coating purity. A very small amount of Al (1.5 wt%) is also detected, which may be attributed to minor contamination during sample preparation or polishing processes. The absence of substrate elements such as Fe suggests that the Ni layer is sufficiently thick to fully cover the underlying substrate in the analyzed region. These results demonstrate that the ELP process produced a dense and relatively uniform Ni coating with high elemental purity and adequate surface coverage. The SEM micrograph in (c) shows a nodular surface morphology typical of electroplated Ni coatings. The EDS analysis confirms that Ni is the dominant element (88.5 wt%), indicating successful Ni deposition. The presence of Cu (11 wt%) is attributed to

the underlying Cu layer or substrate influence, while trace amounts of sulfur (S) and iron (Fe) originate from bath additives and substrate contribution [93,94].

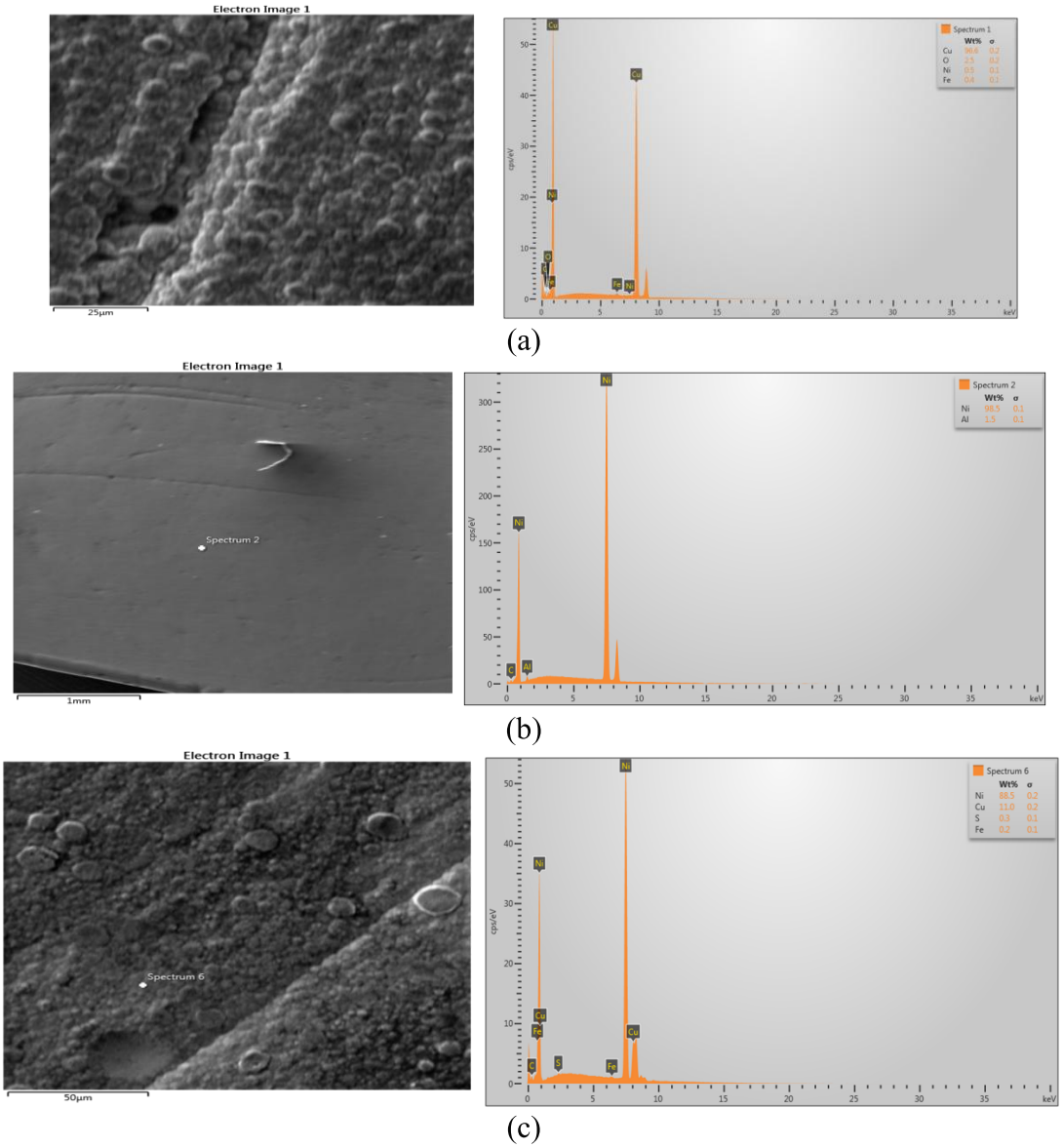

Figure 13 The SEM, EDX analysis of (a) Cu (b)Ni (c) Cu-Ni coating.

5. CONCLUSIONS

1. The thickness of the Cu, Ni & Cu-Ni layers plated on low-carbon steel gradually increased with increasing ELP time, with the greatest thickness achieved at 30 min.
2. Investigations indicate that the surface roughness of the coating (Cu, Ni, and Cu-Ni) increases with increasing layer time and thickness, which relates to electroplating conditions in terms of temperature and current.
3. The results reveal that the morphology of the grown film is layer by layer, and films with plating thicknesses up to 30 min were mainly amorphous.

4. The Cu-Ni bilayer coating showed Vickers hardness values higher than the substrate made of low carbon steel.
5. The successful coating deposition process was demonstrated by the development of discrete diffraction peaks in X-ray diffraction (XRD) analysis, confirming the production of the intended phases with increasing coating time, compared to the uncoated sample.
Scanning electron microscope (SEM) images showed a uniform and dense surface morphology at high thickness, which is evidence of layer integrity. These results indicate the effectiveness of the coating process in improving surface properties, which in turn will improve corrosion resistance in the future.

References

[1] D. Kennedy, Y. Xue, E. Mihaylova, Surf. Eng. 21 (2005) 1. https://doi.org/10.1179/174329405X21955
[2] P. Martin, Surf. Eng. 28 (2012) 1. https://doi.org/10.1179/1743294411Y.0000000050
[3] N.H. Obaeed, W.K. Hamdan, Mater. Today Proc. 81 (2023) 123. https://doi.org/10.1016/j.matpr.2023.02.123
[4] H.K. Mohammed et al., AIP Conf. Proc. 3350 (2025) 020001. https://doi.org/10.1063/5.0200001
[5] H.A. Ali et al., AIP Conf. Proc. 2806 (2023) 020015. https://doi.org/10.1063/5.0134567
[6] R.M. Miranda et al., Mater. Des. 65 (2015) 1021. https://doi.org/10.1016/j.matdes.2014.10.012
[7] H.K. Mohammed et al., AIP Conf. Proc. 3002 (2024) 020010. https://doi.org/10.1063/5.0180002
[8] A.S. Abbas et al., Corros. Sci. 212 (2023) 110918. https://doi.org/10.1016/j.corsci.2022.110917
[9] M.S. Nsaif et al., J. Phys. Conf. Ser. 2857 (2024) 012055. 8https://doi.org/10.1088/1742-6596/2857/1/012056
[10] M.S. Nsaif et al., AIP Conf. Proc. 3321 (2025) 020042. 2https://doi.org/10.1063/5.0289758
[11] M.J. Kadhim et al., IOP Conf. Ser. Mater. Sci. Eng. 518 (2019) 032023. https://doi.org/10.1088/1757-899X/518/3/032022
[12] N. Kanani, Surf. Coat. Technol. 200 (2005) 1. https://doi.org/10.1016/j.surfcoat.2005.02.121
[13] I. Hutchings, P. Shipway, Wear 302 (2013) 1. https://doi.org/10.1016/j.wear.2013.01.002
[14] D. Oloruntoba et al., Surf. Eng. 29 (2013) 1. https://doi.org/10.1179/1743294412Y.0000000101
[15] I. Saeki et al., ISIJ Int. 60 (2020) 2031. https://doi.org/10.2355/isijinternational.ISIJINT-2020-124
[16] R. Alzinkee et al., Case Stud. Chem. Environ. Eng. 8 (2024) 100412. https://doi.org/10.1016/j.cscee.2024.100413
[17] K.A. Sukkar, Eng. Technol. J. 35 (2017) 1. https://doi.org/10.30684/etj.35.10A.2
[18] A.S. Abbas et al., J. Pet. Res. Stud. 12 (2022) 290. https://doi.org/10.52716/jprs.v12i1.291
[19] S.A. Salih et al., Eng. Fail. Anal. 34 (2013) 1. https://doi.org/10.1016/j.engfailanal.2013.07.014
[20] B.A. Abdulhussein et al., Chem. Pap. 77 (2023) 1533. https://doi.org/10.1007/s11696-022-02571-8
[21] Y.D. Gamburg, G. Zangari, Electrochim. Acta 54 (2009) 1. https://doi.org/10.1134/S1023193516090031
[22] D.A. Snow, Reliab. Eng. Syst. Saf. 88 (2005) 1. 10.1109/TR.2010.2052193
[23] B. Fotovvati et al., J. Manuf. Mater. Process. 3 (2019) 28. 10.3390/jmmp3010028
[24] C.P. Thornton, J. Archaeol. Sci. 34 (2007) 1. https://doi.org/10.1146/annurev-anthro-092611-145719
[25] M.V. Postigo, Electrochim. Acta 56 (2011) 1. https://doi.org/10.1016/j.electacta.2011.07.011
[26] W. Giurlani et al., Coatings 8 (2018) 260. https://doi.org/10.1149/ma2018-01/3/260
[27] L.M.L. de Oliveira et al., Quim. Nova 48 (2025) e20250103. https://doi.org/10.1002/elan.200503237

[28] M. Liu et al., Surf. Coat. Technol. 286 (2016) 285. https://doi.org/10.1007/s35724-025-1654-2
[29] W.D. Callister Jr et al., Mater. Sci. Eng. A 527 (2010) 1. https://doi.org/10.1007/s12598-014-0268-5
[30] J.R. Davis, Mater. Sci. Eng. A 287 (2000) 1. https://doi.org/10.1557/PROC-168-145
[31] A. Wiranata, P.D. Setyawan, Mater. Today Proc. 63 (2022) 46. https://jurnal.unram.ac.id/index.php/empd/article/view/1495
[32] S. Çölmekçi et al., Thin Solid Films 727 (2021) 138661. https://doi.org/10.1016/j.tsf.2021.138661
[33] C.G. Levi, Surf. Coat. Technol. 201 (2007) 2071. https://doi.org/10.1108/DPM-12-2025-0433
[34] H. K. Aity, E. Dhahri, M. Rasheed. Ceram. Int. 50 (2024) part B 54666. https://doi.org/10.1016/j.ceramint.2024.10.324
[35] H. K. Aity, M. Rasheed, E. Dhahri, A. A. Hateef, T. Saidani, Journal of Materials Science, 61 (2026) 6226. https://doi.org/10.1007/s10853-026-12241-w
[36] I. Alshalal, H. M. I. Al-Zuhairi, A. A. Abtan, M. Rasheed, M. K. Asmail. J. Mech. Behav. Mater. 32 (2023) 1. https://doi.org/10.1515/jmbm-2022-0280
[37] I.M. Mohammed, M. Rasheed, AIP Conf. Proc. 3321 (2025) 020026. https://doi.org/10.1063/5.0289719
[38] M. A. Sarhan, S. Shihab, B. E. Kashem, M. Rasheed, J. Phy.: Conf. Ser., 1879 (2021) 022122. https://doi.org/10.1088/1742-6596/1879/2/022122
[39] M. Enneffatia, M. Rasheed, B. Louati, K. Guidara, S. Shihab, R. Barillé, J. Phys.: Conf. Ser. 1795 (2021) 012050. https://doi.org/10.1088/1742-6596/1795/1/012050
[40] M. M. Najim, B. A. Yousif, M. RASHEED, Experimental and Theoretical NANOTECHNOLOGY, 10 (2026) 551. https://doi.org/10.56053/10.2.551
[41] M. M. Najim, B. A. Yousif, M. RASHEED, Experimental and Theoretical NANOTECHNOLOGY, 10 (2026) 627. https://doi.org/10.56053/10.2.627
[42] M. Rasheed et al., J. Phys.: Conf. Ser. 1999 (2021) 012080. https://doi.org/10.1088/1742-6596/1999/1/012080
[43] M. RASHEED, A. Khaleefah, Materials Chemistry and Physics, 353 (2026) 132112. https://doi.org/10.1016/j.matchemphys.2026.132112
[44] M. Rasheed, et al., J. Adv. Biotechnol. Exp. Ther. 6 (2023) 495. https://doi.org/10.5455/jabet.2023.d144
[45] M. Rasheed, I. Alshalal, A.A. Ashed, M.A. Sarhan, A.S. Jaber, Indones. J. Electr. Eng. Comput. Sci. 33 (2024) 653. https://doi.org/10.11591/ijeecs.v33.i1.pp653-660
[46] M. Rasheed, M. N. Mohammedali, F. A. Sadiq, M. A. Sarhan, T. Saidani. J. Optics (New Delhi. Print) 54 (2024) 3490. https://doi.org/10.1007/s12596-024-01928-5
[47] M. Rasheed, M. Nuhad Al-Darraji, S. Shihab, A. Rashid, T. Rashid. J. Phys.: Conf. Ser. 1963 (2021) 012058. https://doi.org/10.1088/1742-6596/1963/1/012058
[48] M. Rasheed, M.N. Al-Darraji, S. Shihab, A. Rashid, T. Rashid, J. Phys.: Conf. Ser. 1963 (2021) 012059. https://doi.org/10.1088/1742-6596/1963/1/012059
[49] M. Rasheed, O. Alabdali, S. Shihab, A. Rashid, T. Rashid, J. Phys.: Conf. Ser. 1999 (2021) 012078. https://doi.org/10.1088/1742-6596/1999/1/012078
[50] M. Rasheed, R. Barillé, J. Non-Cryst. Solids., 476 (2017) 1. https://doi.org/10.1016/j.jnoncrysol.2017.04.027
[51] M. Rasheed, R. Barillé, Opt. Quantum Electron. 49 (2017). https://doi.org/10.1007/s11082-017-1030-7
[52] M. Rasheed, S. Shihab, O. Alabdali, A. Rashid, T. Rashid, J. Phys.: Conf. Ser. 1999 (2021) 012077. https://doi.org/10.1088/1742-6596/1999/1/012077

[53] M. Rasheed, SuhaShihab, O. Alabdali, H. H. Hassan, J. Phys. Conf. Ser., 1879 (2021) 032113. https://doi.org/10.1088/1742-6596/1879/3/032113
[54] M. Sellam, M. Rasheed, S. Azizi, T. Saidani. Ceram. Int. 50 (2024) 20917. https://doi.org/10.1016/j.ceramint.2024.03.094
[55] M. T. Mohammed, H. A. Hussein, and A. H. Lafta, "Investigation of microstructure and industrial performance of aluminium–aluminium nitrides nanocomposites produced by stir-casting technique," Advances in Materials and Processing Technologies, pp. 1–12, Aug. 2025, doi: https://doi.org/10.1080/2374068x.2025.2546435
[56] N. Assoudi et al. Opt. Quant. Electron. 54 (2022) 9. https://doi.org/10.1007/s11082-022-03927-x
[57] N. Ben Azaza et al., Opt. Mater., 96 (2019) 109328. https://doi.org/10.1016/j.optmat.2019.109328
[58] O. Alabdali, S. Shihab, M. Rasheed, T. Rashid. 3rd inter. Scient. conf. alkafeel univ. (ISCKU 2021) 2386 (2022) 050019. https://doi.org/10.1063/5.0066860
[59] R. Jalal, S. Shihab, M.A. Alhadi, M. Rasheed, J. Phys.: Conf. Ser. 1660 (2020) 012090. https://doi.org/10.1088/1742-6596/1660/1/012090
[60] R.S. Mahmood et al. J. Mech. Behav. Mater. 34 (2025) 1. https://doi.org/10.1515/jmbm-2025-0040
[61] S. S. Batros, M. Rasheed, H. K. Aity, A. A. Hatef, T. Saidani, Materials Chemistry and Physics, 355 (2026) 132243. https://doi.org/10.1016/j.matchemphys.2026.132243
[62] S. Shihab, M. Rasheed, O. Alabdali, A.A. Abdulrahman, J. Phys.: Conf. Ser. 1879 (2021) 022120. https://doi.org/10.1088/1742-6596/1879/2/022120
[63] T. Rashid, M. M. Mokji, M. Rasheed. J. Optics 54 (2024) 3490. https://doi.org/10.1007/s12596-024-02080-w
[64] T. Rashid, M.M. Mokji, M. Rasheed, J. Mech. Behav. Mater. 34 (2025) 77. https://doi.org/10.1515/jmbm-2025-0074
[65] T. Saidani, M. Rasheed, I. Alshalal, A.A. Rashed, M.A. Sarhan, R. Barillé, Res. Eng. Struct. Mater. 10 (2024) 743. http://dx.doi.org/10.17515/resm2023.21ma0922rs
[66] T. Saidani, S. Mokhtari, M. Rasheed, H. Lahmar, M. Trari, Journal of the Indian Chemical Society, 103 (2026) 102499. https://doi.org/10.1016/j.jics.2026.102499
[67] Z. S. Ahmed, M. RASHEED, H. S. Ahmed, Experimental and Theoretical NANOTECHNOLOGY, 10 (2026) 329. https://doi.org/10.56053/10.s.329
[68] Z. S. Ahmed, M. RASHEED, H. S. Ahmed, Experimental and Theoretical NANOTECHNOLOGY, 10 (2026) 343. https://doi.org/10.56053/10.s.343
[69] A. A. Hateef, E. Dhahri, M. Rasheed, H. Kadhim, Z. Abbas, N. Hassan, Physics and Chemistry of Solid State, 25 (2024) 801. https://doi.org/10.15330/pcss.25.4.801-810
[70] A. Boumezoued, K. Guergouri, Régis Barillé, Rechem Djamil, Mourad Zaabat, M. Rasheed, J. Alloys Compd. 791 (2019) 550. https://doi.org/10.1016/j.jallcom.2019.03.251
[71] A. I. A. Ali, M. RASHEED, Experimental and Theoretical NANOTECHNOLOGY, 10 (2026) 277. https://doi.org/10.56053/10.s.277
[72] A. I. A. Ali, M. RASHEED, Experimental and Theoretical NANOTECHNOLOGY, 10 (2026) 239. https://doi.org/10.56053/10.s.239
[73] A. Jaber, M. Ismael, T. Rashid, M. A. Sarhan, M. Rasheed, I. M. Sala. Eureka: Phys. Eng. 4 (2023) 29. https://doi.org/10.21303/2461-4262.2023.002770
[74] A. Keziz, M. Heraiz, F. Sahnoune, M. Rasheed, Ceram. Int. 49 (2023) 32989. https://doi.org/10.1016/j.ceramint.2023.07.275
[75] A. Keziz, M. Heraiz, M. RASHEED, A. Oueslati. Mater Chem. Phys. 325 (2024) 129757. https://doi.org/10.1016/j.matchemphys.2024.129757

Exp. Theo. NANOTECHNOLOGY 10 (2026) 925-944
[76] A. Khaleefah, M. RASHEED, Experimental and Theoretical NANOTECHNOLOGY, 10 (2026) 289. https://doi.org/10.56053/10.s.289.
[77] A. R. J. Katae, H. H. Hussein, A. S. Jaber, M. A. Sarhan, M. RASHEED, Experimental and Theoretical NANOTECHNOLOGY, 10 (2026) 357. https://doi.org/10.56053/10.s.357
[78] A. R. J. Katae, H. H. Hussein, A. S. Jaber, M. A. Sarhan, M. RASHEED, Experimental and Theoretical NANOTECHNOLOGY, 10 (2026) 795. https://doi.org/10.56053/10.2.795
[79] A. Raghdi, M. Heraiz, M. Rasheed, A. Keziz, Journal of the Indian Chemical Society, 101 (2024) 101413. https://doi.org/10.1016/j.jics.2024.101413
[80] A. Zubaidi, L.M. Asaad, I. Alshalal, M. Rasheed, J. Mech. Behav. Mater. 32 (2023) 1. https://doi.org/10.1515/jmbm-2022-0302
[81] A.H. Ali, A.S. Jaber, M.T. Yaseen, M. Rasheed, O. Bazighifan, T.A. Nofal, Complexity 2022 (2022) 1. https://doi.org/10.1155/2022/9367638
[82] A.J. Hussein, M.N. Al-Darraji, M. Rasheed, M.A. Sarhan, IOP Conf. Ser.: Earth Environ. Sci. 1262 (2023) 022007. https://doi.org/ 10.1088/1755-1315/1262/2/022007
[83] A.J. Hussein, M.N. Al-Darraji, M. Rasheed, M.A. Sarhan, IOP Conf. Ser.: Earth Environ. Sci. 1262 (2023) 022005. https://doi.org/10.1088/1755-1315/1262/2/022005
[84] D. Bouras, M. Rasheed, Opt. Quantum Electron. 54 (2022) 12. https://doi.org/10.1007/s11082-022-04161-1
[85] D. Kherifi, A. Keziz, M. Rasheed, A. Oueslati. Ceram. Int. 50 part A (2024) 30175. https://doi.org/10.1016/j.ceramint.2024.05.317
[86] E. Arif, R. Jamal, M. RASHEED, Experimental and Theoretical NANOTECHNOLOGY, 10 (2026) 453. https://doi.org/10.56053/10.2.453
[87] E. Kadri, K. Dhahri, R. Barillé, M. Rasheed. Phase Transi. 94 (2021) 65. https://doi.org/10.1080/01411594.2020.1832224
[88] F. Boudou, A. Belakredar, A. Berkane, M. Rasheed. Not. Sci. Biol. 17 (2025) 12183. https://doi.org/10.55779/nsb17212183
[89] F. Boudou, A. Guendouzi, A. Belkredar. M. Rasheed, Not. Sci. Biol. 16 (2024) 13837. https://doi.org/10.55779/nsb16211837
[90] F. Boudou, et al., Not. Sci. Biol. 17 (2025) 12593. https://doi.org/10.55779/nsb17312593
[91] F. Dkhilalli, S. M. Borchani, M. Rasheed, R. Barille, K. Guidara, M. Megdiche, J. Mater. Sci. Mater. Electron, 29 (2018) 6297. https://doi.org/10.1007/s10854-018-8609-z.
[92] H. A. Hussein, S. G. Hussein, and Bassim Bachy, "Evaluation of the Effect of Nano Al_2O_3 Additive on Al-Si-Cu Alloys Performance Produced by Squeeze Casting and High Pressure Die Castings: Experimentation and Mathematical Modeling," Mathematical Modelling and Engineering Problems, vol. 12, no. 7, pp. 2234–2244, Jul. 2025, doi: https://doi.org/10.18280/mmep.120704
[93] M. Rasheed, O. Alabdali, S. Shihab, J. Phy.: Conf. Ser. 1879 (2021) 032120. https://doi.org/10.1088/1742-6596/1879/3/032120
[94] M. Rasheed, O.Y. Mohammed, S. Shihab, A. Al-Adili, J. Phys.: Conf. Ser. 1795 (2021) 012043. https://doi.org/10.1088/1742-6596/1795/1/012043

Exp. Theo. NANOTECHNOLOGY 10 (2026) 925-944